The Mechanics of FtsZ Fibers

Daniel J. Turner,[†‡] Ian Portman,[§] Timothy R. Dafforn,[¶] Alison Rodger,[†‖**] David I. Roper,[§] Corinne J. Smith,[§] and Matthew S. Turner[‡††*]

[†]Molecular Organisation and Assembly in Cells Doctoral Training Centre, [‡]Department of Physics, and [§]Department of Life Sciences, University of Warwick, Coventry, United Kingdom; [¶]School of Biosciences, University of Birmingham, Birmingham, United Kingdom; [‖]Department of Chemistry, **Warwick Centre for Analytical Science, and [††]Complexity Centre, University of Warwick, Coventry, United Kingdom

ABSTRACT Inhibition of the Fts family of proteins causes the growth of long filamentous cells, indicating that they play some role in cell division. FtsZ polymerizes into protofilaments and assembles into the Z-ring at the future site of the septum of cell division. We analyze the rigidity of GTP-bound FtsZ protofilaments by using cryoelectron microscopy to sample their bending fluctuations. We find that the FtsZ-GTP filament rigidity is $\kappa = 4.7 \pm 1.0 \times 10^{-27}$ Nm^2, with a corresponding thermal persistence length of $l_p = 1.15 \pm 0.25$ μm, much higher than previous estimates. In conjunction with other model studies, our new higher estimate for FtsZ rigidity suggests that contraction of the Z-ring may generate sufficient force to facilitate cell division. The good agreement between the measured mode amplitudes and that predicted by equipartition of energy supports our use of a simple mechanical model for FtsZ fibers. The study also provides evidence that the fibers have no intrinsic global or local curvatures, such as might be caused by partial hydrolysis of the GTP.

INTRODUCTION

Inhibiting the function of the filamentous temperature-sensitive family of proteins causes the growth of long filamentous cell shapes in bacteria (1). Because their inactivation is not directly lethal to the cell, this indicates that each protein plays some role in cell division. One such protein is FtsZ, the prokaryotic homolog to tubulin (2,3). This is believed to be the major cytoskeletal protein involved in bacterial cell division. FtsZ assembles into a ring, known as the Z-ring (4), which attaches to the membrane around the longitudinal midpoint of the cell, and contracts to divide the cell (5).

The formation of the Z-ring is facilitated by the ability of FtsZ to bind to GTP, which enables polymerization of FtsZ, resulting in the creation of straight protofilaments (6,7). Many of these straight protofilaments are then bundled together to form the Z-ring. FtsZ also exhibits a GTPase domain that allows it to hydrolyze GTP to GDP (8). Polymers formed by the binding of FtsZ to GDP have an intrinsically curved conformation (9), with a 22° bend between FtsZ monomers, which leads to a mini ring of 16 subunits with an outside diameter of 23 nm (10). It is postulated that the contraction of the Z-ring that occurs during cell division may be generated by the hydrolysis of GTP to GDP bound within the FtsZ protofilaments (11), which then bends as in the FtsZ-GDP filaments. There is also recent evidence of a second curved conformation of FtsZ protofilaments, which does not seemingly require GTP hydrolysis (3). Atomic force microscopy images of FtsZ-GTP protofilaments on mica appear to show curvatures with a diameter of ~200 nm (12,13). Surface interactions may play an important role here.

To build a qualitative model of the mechanics of this process, one would like to know as much as possible about the physical properties of the FtsZ protofilaments that comprise the Z-ring. Here, we estimate the rigidity, κ, of FtsZ protofilaments by studying their fluctuations at thermal equilibrium, as well as their persistence length, l_p. The two are related by the equation $l_p = \kappa / k_B T$ (where k_B is the Boltzmann constant and T the absolute temperature). The rigidity could be used to calculate the restoring force exerted by such a protofilament due to a given bending strain. This has obvious implications for studying the forces generated by the contraction of the Z-ring in bacteria, where previous estimates have been used in models to try and determine whether the force generated by Z-ring contraction could be sufficient to facilitate cell division (14,15).

Previous articles on the study of FtsZ-GTP protofilaments reported values for the persistence length of 54 ± 2 nm (16) (The authors give an alternative estimate of the persistence length $l_p = 162 \pm 6$ nm in the case that the fibers are not confined to a thin (two-dimensional) film. However, the method employed (17) to make these estimates was developed for use when a separate measure of the contour length was available, e.g., DNA with a known sequence length, otherwise some care must be taken to estimate this from its projection.) and 180 nm (18). However, the cryo-electron microscopy (cryo-EM) images presented in these articles show many FtsZ filaments in contact with each other, raising the possibility that their conformations could be perturbed by these contacts. The forces that the filaments would then impose on one another could cause them to bend more than they would when isolated and at equilibrium,

Submitted July 28, 2011, and accepted for publication January 11, 2012.

*Correspondence: m.s.turner@warwick.ac.uk

Editor: Edward Egelman.

0006-3495/12/02/0731/8 $2.00

doi: 10.1016/j.bpj.2012.01.015

resulting in an underestimate of the persistence length (and rigidity) of FtsZ-GTP protofilaments. We examine the effects of these nonthermal forces below. In another study, where FtsZ protofilaments were deposited onto a mica surface and visualized using atomic force microscopy (19), the fibers were long enough to resemble flexible, thread-like filaments rather than the shorter (and hence apparently more rod-like) fibers that we report on below. An estimate is given for the persistence length for FtsZ fibers on mica of 4 μm (19), ~25 times greater than the larger of the previous literature estimates. However, it must be noted that the study involved FtsZ fibers adsorbed onto a mica surface under conditions that are therefore very different to those found in vivo or in solution (immediately before freezing). For this reason, we do not believe that these experiments (19) give a reliable estimate of the FtsZ filament rigidity in vivo.

In our own studies, we use cryoEM to acquire images of dilute solutions of FtsZ-GTP protofilaments. We then search the images for protofilaments that are not in contact with anything else, extract the contours of the protofilaments, transform these contours to a Fourier sine series, and then use the amplitudes of the Fourier modes to calculate the rigidity and persistence length of the naturally straight protofilaments. By rapidly freezing the sample, the images we obtain are a snapshot of the protofilament conformations at the temperature at which they were prepared (see Materials and Methods). By collecting and analyzing many such snapshots of fluctuating fibers, we are able to estimate the mean amplitude of these fluctuations and, using the principle of equipartition of energy, the fiber rigidity.

THEORY

The total bending energy, E, of a uniform fiber of length L in the absence of external forces is written (20):

$$E = \frac{\kappa}{2}\int_0^L \frac{\partial^2 \mathbf{u}}{\partial z^2}\cdot\frac{\partial^2 \mathbf{u}}{\partial z^2}\,dz, \tag{1}$$

where the vector $\mathbf{u}(z)$ represents normal deviations from the fiber axis (z), defined to be a straight line that passes through the fiber ends. A sufficient condition for our method to be accurate to leading order in the fiber displacements is that $|d\mathbf{u}/dz|<<1$ everywhere. Here, we are only able to measure fluctuations projected onto the x-z focal plane, hence we decompose the above into $E = E^{(x)} + E^{(y)}$ with u_x the x component of $u(z)$:

$$E^{(x)} = \frac{\kappa}{2}\int_0^L \left(\frac{\partial^2 u_x}{\partial z^2}\right)^2 dz, \tag{2}$$

and similarly for $E^{(y)}$. The resulting factorization of the distributions of u_x and u_y means that they can be considered to vary independently for the small deviations of interest to us here.

In this article, we discuss the use of cryo-EM to visualize FtsZ fibers suspended in a very thin film of aqueous buffer solution before rapid freezing. Due to the limited film thickness the fluctuations of the filaments in the y direction, normal to the surface(s) of the film, may very well be strongly constrained by the presence of the air interfaces. In particular, we do not see any fibers end-on for the simple reason there is simply not enough room for them to orientate that way without piercing, or significantly distorting, the air-interface(s) of the film. However, because the in-plane and out-of-plane fluctuations are completely decoupled (their probability distributions factorize) means that we can still have confidence that we can extract information on the fiber mechanics from an analysis of the in-plane (x-z) fluctuations alone.

Expressed in its Fourier components, the displacement of such a fiber in the x direction, $u_x(z)$, can be written

$$u_x(z) = \sum_{n=1}^{\infty} a_n \sin\left(\frac{\pi n z}{L}\right), \tag{3}$$

where a_n is the amplitude of the nth Fourier mode. Substituting Eq. 3 into Eq. 2, integrating, and exploiting the orthogonality of Fourier modes, we find the energy in each Fourier mode $E_n^{(x)}$:

$$E^{(x)} = \frac{\pi^4\kappa}{4L^3}\sum_{n=1}^{\infty} n^4 a_n^2 = \sum_{n=1}^{\infty} E_n^{(x)}. \tag{4}$$

By the principle of equipartition of energy (21), $\langle E_n^{(x)}\rangle = k_B T/2$, thus the mean squared Fourier amplitude is

$$\langle a_n^2\rangle = \frac{2k_B T L^3}{\kappa\pi^4 n^4}. \tag{5}$$

A similar approach has previously been used as the starting point for determining the rigidity of other fibers with a naturally straight conformation, such as sickle cell hemoglobin (22).

We expect some error in our measurements of the mode amplitudes, which we shall denote by $\tilde{a}_n$. We can write this as $\tilde{a}_n = a_n + \delta a_n$, with δa_n a normally distributed noise contribution, which we assume to be unbiased so that $\langle\delta a_n\rangle = 0$. To estimate the variance of δa_n, we analyze the error we make in determining the position, $u_x(z)$, of the fiber. We can also decompose our measured position $\tilde{u}_x(z)$ into the sum of its actual position, $u_x(z)$, and a noise term $\delta u_x(z)$, which we also shall assume is normally distributed with $\langle\delta u_x(z)\rangle = 0$ and variance r^2. Due to the linearity of the Fourier transform, we can use the inverse transform to obtain δa_n in terms of $\delta u_x(z)$:

$$\delta a_n = \frac{2}{L}\int_0^L \delta u_x(z)\sin\frac{\pi n z}{L}\,dz. \tag{6}$$

With our choice of δu_x, $\langle \delta a_n \rangle = 0$ and the variance of δa_n is equal to $\langle \delta a_n^2 \rangle$, giving

$$\langle \delta a_n^2 \rangle = \frac{4}{L^2} \int_0^L \int_0^L \langle \delta u_x(z) \delta u_x(z') \rangle \sin \frac{\pi n z}{L} \sin \frac{\pi n z'}{L} dz dz'. \quad (7)$$

We now assume that $\langle \delta u_x(z) \delta u_x(z') \rangle = r^2$ if $|z - z'| < b/2$, where $b = 0.462$ nm is the width of the pixels in our images of the fibers, otherwise $\langle \delta u_x(z) \delta u_x(z') \rangle = 0$. Furthermore, by assuming that $\sin \pi n z/L$ is approximately constant over a length b, we are now able to solve the integral in Eq. 7 to obtain

$$\langle \delta a_n^2 \rangle = \frac{2br^2}{L}. \quad (8)$$

Although we have provided a direct motivation for the physical interpretation of the parameters that appear in Eq. 8, because r remains undetermined we are effectively allowing for a rather general contribution from any (Gaussian) measurement noise. We will later estimate r by comparison with experimental data.

Now, we can write the probability density function for mode amplitude $\tilde{a}_n$ as

$$P(\tilde{a}_n) = \mathcal{N} \int_{-\infty}^{\infty} \left(e^{-\alpha \left(\tilde{a}_n - \delta a_n \right)^2 - \beta \delta a_n^2} \right) d\delta a_n, \quad (9)$$

where $\mathcal{N}$ is a normalization constant, $\alpha = l_p n^4 \pi^4 / 4L^3$ and $\beta = L/4br^2$. By setting $A_n = \delta a_n - \alpha \tilde{a}_n / \alpha + \beta$, we can rearrange this to the following:

$$P(\tilde{a}_n) = \mathcal{N} \int_{-\infty}^{\infty} \left(e^{-(\alpha+\beta) A_n^2 - \frac{\alpha\beta \tilde{a}_n^2}{\alpha+\beta}} \right) dA_n. \quad (10)$$

This integral is now in a form in which it can be solved analytically to find the value of $\mathcal{N}$. Doing so, we obtain the following final form for $P(\tilde{a}_n)$:

$$P(\tilde{a}_n) = \sqrt{\frac{\gamma}{\pi}} e^{-\gamma \tilde{a}_n^2}, \quad (11)$$

$$\gamma = \frac{\alpha\beta}{\alpha+\beta} = \frac{l_p n^4 \pi^4 L}{4\left(L^4 + l_p n^4 \pi^4 b r^2\right)}. \quad (12)$$

We have collected data from a series of cryoelectron micrographs of FtsZ fibers by determining the contour of each fiber and using the Fourier decomposition to obtain $\tilde{a}_n$ for different modes n. Using the whole data set of values of $\tilde{a}_n$ and L for multiple Fourier modes n from each fiber, we can then generate estimates for l_p and r by maximizing the product of P over the whole set of fibers, which is the likelihood function of l_p and r given the observed values of $\tilde{a}_n$, L, and n.

The logarithm is a monotonically increasing function; therefore, the point (l_{pmax}, r_{max}) at which the maximum likelihood is attained is the same point at which the maximum of the logarithm of this product occurs, known as the log-likelihood. Because $\log(\prod_i x_i) = \sum_i \log(x_i)$, we can also attain the same estimates by maximizing the log-likelihood expressed as the following sum over all of our measurements with respect to l_p and r.

$$\sum_i \log\left(P_i(l_p, r)\right), \quad (13)$$

where the probability density $P_i(l_p, r)$ is found using a particular set of measurements i.

We believe that our approach, in which we analyze the (small) mode amplitudes directly, represents an improvement (for short/stiff fibers) over the method of (17), in which small variations of the projected end-to-end distance are measured. For stiff fibers the latter method has the disadvantage that one must identify a small signal (variations in distance) from a large background (roughly the fiber contour length), although it has advantages for long/floppy fibers as our approach fails whenever $|d\mathbf{u}/dz| \gtrsim 1$.

MATERIALS AND METHODS

Expression and purification of FtsZ

To collect data for analysis, it was necessary to produce monomeric FtsZ. This method for the expression and purification of FtsZ is derived from that given by Mukherjee and Lutkenhaus (23,24). To overexpress FtsZ, *Escherichia coli* competent cells B834 were transformed with the plasmid pETFtsZ. 10 ml of LB containing 0.1 mg/ml ampicillin were then inoculated with a fresh colony of the transformed cells, incubated overnight at 37°C, and then diluted into 3 liters of LB. The culture was then grown at 37°C until $OD_{600} = 0.4$, at which point we induced it with 1 mM isopropyl-β-D-thiogalactopyranoside and let it grow for 3 more hours. The culture was harvested by centrifugation, and the cell pellet was resuspended in buffer A (50 mM Tris-HCl, pH 7.9, 50 mM KCl, 1 mM EDTA, and 10% glycerol) and lysed by sonication. Cell debris was removed by centrifugation. The supernatant was then collected and 30% ammonium sulfate (16.6 g/100 ml of extract) was slowly added with stirring for 20 min. The ammonium sulfate precipitate was then recovered by centrifugation and resuspended in buffer A, which was then dialyzed overnight against buffer A. FtsZ is extracted by ion exchange chromatography using a DEAE-Sepharose column. Sodium dodecyl sulfate polyacrylamide gel electrophoresis gel was used to locate fractions containing high concentrations of FtsZ. These fractions were pooled and dialyzed overnight against buffer A, and then stored at −80°C.

Cryo-EM of FtsZ-GTP protofilaments

FtsZ at 11 μM was incubated for 15 min at 20°C in the polymerization buffer (50 mM MES-KOH, pH 6.5, 50 mM KCl, and 10 mM $MgCl_2$) (25). The polymerization reaction was initiated by the addition of 0.2 mM GTP, and 2 min elapsed before 5 μl of sample was added to a carbon grid and rapidly frozen by plunging into liquid ethane at approximately −170°C. The grid was observed using a Jeol (Tokyo, Japan) 2011

Transmission Electron Microscope fitted with a Gatan (Pleasanton, CA) UltraScan 1000 camera. Images were acquired of ice-filled holes in the grid containing one or more isolated FtsZ-GTP protofilaments. Fig. 1 shows one of the cryoelectron micrographs of FtsZ-GTP protofilaments we obtained during our work, which was then used in our analysis. The filaments are ~4–5 nm wide and range in length from ~100 to 800 nm. The grids used in our experiments were purchased from Agar Scientific (Stansted, UK).

Extraction of contours from images

Once an isolated FtsZ-GTP protofilament had been found within an image, MacBiophotonics ImageJ was used to rotate the image so that the fiber axis was horizontal, to crop the image so that the ends of the fiber were located at either end of the image, and then to apply a Gaussian filter to facilitate subsequent analysis. This process is illustrated in Fig. 2. Furthermore, measurement tools within ImageJ were used to ascertain the distance between the two ends of the fiber. Each of these processed grayscale images were imported to Wolfram Mathematica as a matrix of values between 0 and 1, representing the intensity of each pixel in the image. Each column of the matrix was then fitted to a column of values representing a standard average fiber cross section by using a sum of least squares method, and in this way the vertical position of the fiber was determined. An interpolation between these locations was then constructed as an approximation to the fiber contour. The Fourier coefficients of this interpolated function were then computed numerically from the inverse of Eq. 3.

RESULTS

As described previously in the Methods section, the expressed monomeric FtsZ was polymerized with the addition of GTP to form fibers in solution. The fibers were then added to a carbon grid, rapidly frozen, and imaged using an electron microscope, producing a series of images including the one shown in Fig. 1. From these images we identified 48 isolated FtsZ-GTP protofilaments (see Fig. 2 for an example) to be analyzed as above, and from these images we determined the length of each fiber as well as the amplitudes of the first 10 Fourier modes (see Table S1 in the Supporting Material). Using these data, we compose the sum described in Eq. 13 and maximize it numerically with respect to l_p and r. By doing so, we obtain the following estimates for these parameters:

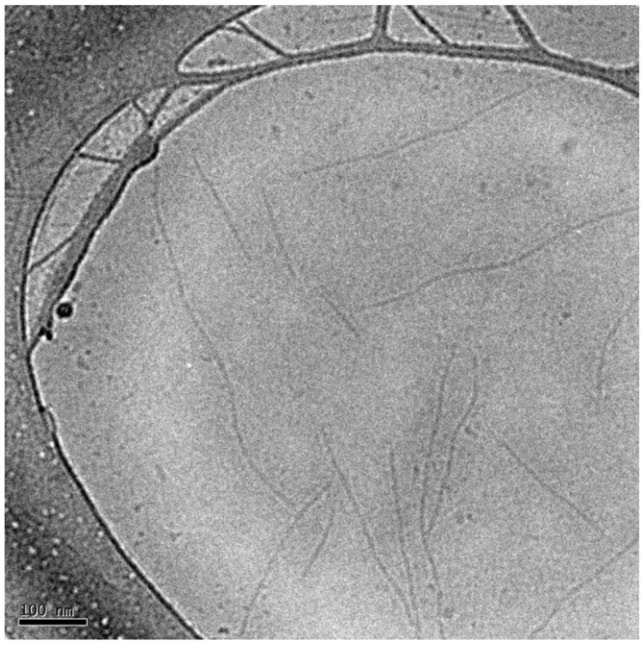

FIGURE 1 Typical cryoelectron micrograph of FtsZ-GTP protofilaments as described in the Materials and Methods section. The scale bar in the image corresponds to a length of 100 nm.

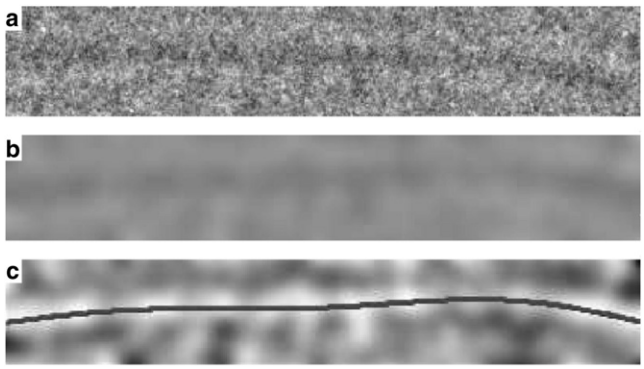

FIGURE 2 Illustration of how we extract the shape of our FtsZ-GTP protofilaments from our images. Starting from the image shown in Fig. 1, we magnify a particular fiber, which is seen not to be interacting with any others, and then crop the image as shown (*a*). The image is then rotated such that the fiber axis is aligned horizontally and a Gaussian filter is applied (*b*). Finally, we obtain a mathematical interpolation for the fiber contour, seen here overlaid on the image (*c*), as described in the text.

$$l_p = 1.15\ \mu\text{m}, \tag{14}$$

$$r = 4.43\ \text{nm}. \tag{15}$$

This estimate for the persistence length of an FtsZ-GTP protofilament gives a corresponding rigidity of $\kappa = 4.67\times10^{-27}\ \text{Nm}^2$.

We can now obtain a 90% confidence region for these estimates. To do so, we first approximate P, the probability density function for a mode amplitude $\tilde{a}_n$, around its maximum by the function p:

$$P(l_p, r) \approx p(l_p, r) = \mathcal{N} e^{-\underline{\psi}^T \cdot B \cdot \underline{\psi}}. \tag{16}$$

Here, $\underline{\psi} = (r, l_p)$, $\mathcal{N}$ is a normalization factor, and B is the Hessian matrix of the second derivatives of $P(l_p, r)$ with respect to r and l_p evaluated at its maximum.

By diagonalizing B we change variables from (r, l_p) to (R, L_P):

$$p(L_P, R) = \frac{1}{\pi} e^{-R^2 - L_P^2}. \tag{17}$$

The 90% confidence region is a circle with radius $\sqrt{R^2 + L_P^2} = c$ in these coordinates. Integrating, we find the probability of L_P and R being in this region is equal to $1 - e^{-c^2}$. Setting this equal to 0.9, corresponding to a

90% confidence region, we obtain $c = 1.52$. Solving $\sqrt{R^2 + L_P^2} = 1.52$ and transforming back to our original variables, this gives us the confidence region shown in Fig. 3. The extreme values of l_p and r within this region are determined numerically, and are 0.91 and 1.40 μm for l_p, and 2.68 and 6.16 nm for r. These ranges represent the error bars on our estimates of l_p and r. Reassuringly, our estimate of r, which quantifies the imprecision in our measurement of fiber position, is approximately equal to the fiber width.

Negatively stained FtsZ fibers

We repeated the analysis described for images obtained using cryo-EM for negatively stained FtsZ filaments, see the Supporting Material. Although we have reservations concerning the extent to which the negative staining could affect the structure and mechanics of the fibers, this exercise is worthwhile as a form of control experiment. The data we gathered are available in Table S2. Using this method, we generated an estimate for their persistence length of $l_p = 1.11$ μm, with $r = 14.5$nm.

DISCUSSION

Agreement between data and model

Our model (see Eq. 1), when combined with our estimates for l_p and r, is in very good agreement with the measured mode amplitudes (and fiber lengths). Fig. 4 is a key result of this study. It shows a plot of the measured values of $\langle \tilde{a}_n^2/L^3 \rangle$ for each mode (with error bars giving the standard error of the mean) versus the theoretical values that one would expect to obtain using our estimates of l_p and r in the following formula, which is obtained by substituting Eq. 5 and Eq. 8 into $\tilde{a}_n = a_n + \delta a_n$, averaging and then rearranging:

$$\left\langle \frac{\tilde{a}_n^2}{L^3} \right\rangle = \frac{2}{l_p n^4 \pi^4} + 2br^2 \left\langle \frac{1}{L^4} \right\rangle. \tag{18}$$

From Fig. 4, it is clear that the combination of our model for the behavior of the FtsZ filaments and the estimates we obtain for l_p and r provides a good explanation for the fluctuations we observed in our electron micrographs. The quality of fit to the theory also provides strong evidence that equipartition of energy is appropriate (the system remains near equilibrium). It also validates our use of the simple mechanical model given in Eq. 1, which describes FtsZ filaments as homogeneous fibers with a groundstate that is straight and characterized by a single mechanical modulus, their rigidity. If FtsZ filaments had a spatially varying rigidity, or regions with intrinsic curvature, a signature would be expected at the corresponding mode amplitude, i.e., a bump in Fig. 4 where the measured value of $\langle \tilde{a}_n^2/L^3 \rangle$ would be higher than expected. This has implications for the kinetics of hydrolysis and depolymerization of these fibers; regions of polymerized GDP-bound FtsZ in the fiber midsection, resulting in a region of increased

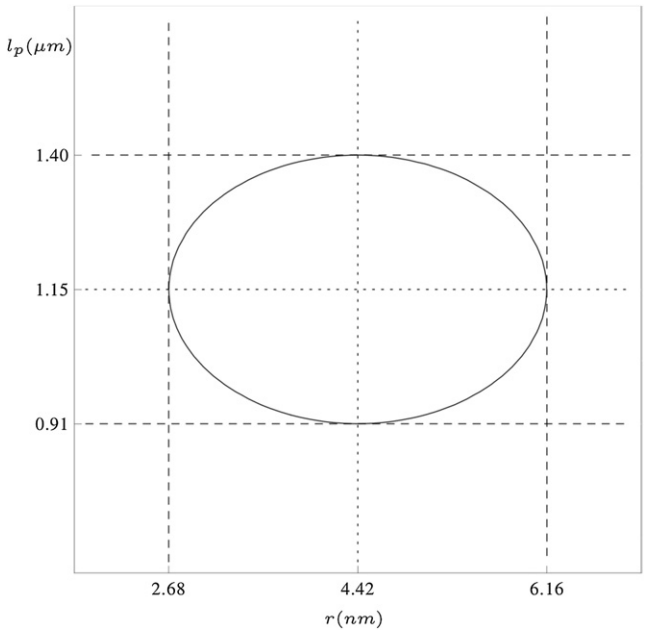

FIGURE 3 For l_p and r the 90% confidence region is shown by the ellipse, determined as described in the text.

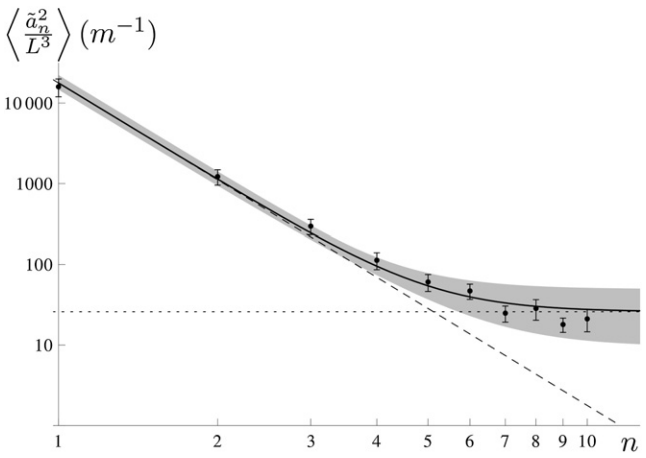

FIGURE 4 Plot showing $\langle \tilde{a}_n^2/L^3 \rangle$ for each Fourier mode n for isolated fibers imaged using cryo-EM. The experimental data from isolated FtsZ-GTP filaments is represented by circular markers with error bars corresponding to the mean $\pm$ standard error. The solid black line represents the theoretical model with our estimates of $l_p = 1.15$ μm and $r = 4.42$ nm. The intercept with the $n = 1$ axis is 1.78×10^4 m^{-1}, which can be identified with $2/l_p\pi^4$ according to Eq. 5, corresponding to $l_p = 1.15$ μm. The gray shaded area represents the set of values for $\langle \tilde{a}_n^2/L^3 \rangle$ which can be obtained using values of l_p and r from within the 90% confidence region shown in Fig. 3. The black dashed line represents the underlying theoretical result from Eq. 5 (in the absence of noise)and has slope -4 on this log-log plot. The black dotted horizontal line represents the contribution of the noise to $\langle \tilde{a}_n^2/L^3 \rangle$, to which the solid black line is asymptotic; the highest modes are always dominated by measurement noise.

curvature (9), would result in a deviation from the power-law behavior seen in Fig. 4. We are not able to rule out small amplitude helicity on length scales corresponding to the noise-dominated regime $n \gtrsim 4$; however, because our estimate of the rigidity is extracted primarily from the first few modes it should be insensitive to the presence of weak helical (nonthermal) bending on these scales. FtsZ-GTP fibers bound to mica have been shown to be curved (12,13). We believe this may be due to surface interactions.

Negatively stained FtsZ fibers

Our estimate for the persistence length calculated from negative stain images of FtsZ fibers lies well within our 90% confidence region for our estimate using cryo-EM seen in Fig. 3. The increase in r implies that we have a slightly greater source of noise in our analysis of the negative stain images. Fig. 5 shows a plot of the measured values of $\langle \tilde{a}_n^2/L^3 \rangle$ for each mode (with error bars giving the standard error of the mean) versus the theoretical values that one would expect to obtain using the estimates of l_p and r from our negative stain images in the formula given in Eq. 18. We can see that there is a good fit between the model and the experimental data obtained from the negatively stained fibers, although it is not quite as strong as the fit observed with the data from the cryo-EM images. Nonetheless, we reiterate that an approach based on cryo-EM of frozen hydrated samples represents the most reliable method of obtaining information on filament rigidities. The fact that the two estimates of the filament mechanics obtained from negatively stained and frozen hydrated samples are so close is potentially useful. It provides evidence that it might be possible to use negatively stained samples more generally to obtain mechanical information, despite our reservations concerning the use of negative staining on general biophysical grounds. It also provides further evidence that we can safely disregard any concerns over the thickness of the buffer film because none are present when we use a negative staining protocol (see the Supporting Material for details).

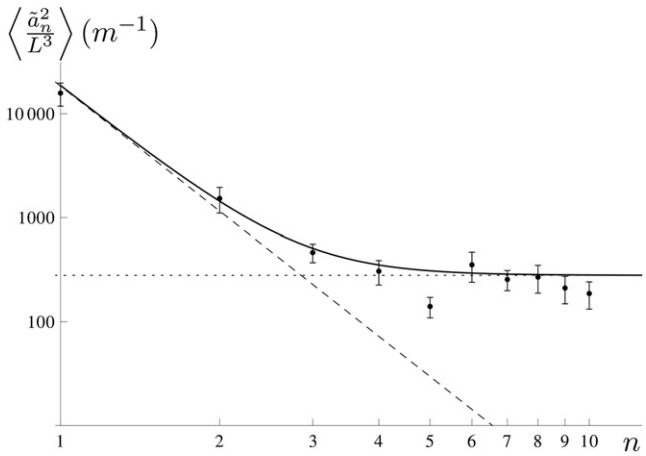

FIGURE 5 Plot showing $\langle \tilde{a}_n^2/L^3 \rangle$ for each Fourier mode n for isolated fibers imaged using negative stain electron microscopy. The experimental data from isolated FtsZ-GTP filaments are represented by circular markers with error bars corresponding to the mean $\pm$ standard error. The solid black line represents the theoretical model with our estimates of $l_p = 1.11$ μm and $r = 14.5$ nm. The dashed and dotted asymptotes have the same meaning as in Fig. 4.

Comparison with previous estimates

A primary result of this work is that our estimate for l_p is significantly greater than those found previously (16,18). For example, Huecas et al. reported a persistence length of ~54 nm, which is <5% of our estimate. It appears that these authors analyzed FtsZ filaments in contact with each other, raising the possibility that their deformation may have been affected by interfiber contacts and not purely due to thermal fluctuations (26). This could have a large effect on the final result, as any forces that the filaments impart on one another could cause them to bend more than they would if isolated, resulting in an underestimation of the persistence length (and rigidity) of FtsZ-GTP protofilaments. These forces could arise, for example, from van der Waals or hydrophobic interactions, or even depletion forces (27).

To quantify the errors that could arise from using nonisolated filaments to estimate rigidity, we applied our analysis to filaments in contact with one another. In this way, we generate alternative (unreliable) estimates of $l_p = 0.49$ μm and $r = 3.61$ nm (see Fig. 6). This is a significant underestimate of FtsZ rigidity by a factor of ~2.3. In the EM image shown in the article by Huecas et al. (16) the concentration of FtsZ fibers seems much higher than ours, leading to more interfiber contacts, potentially exacerbating the discrepancy.

The discrepancy between these two estimates of l_p actually provides a qualitative measure of the strength of the attractive interactions between FtsZ fibers of about $k_B T$ per persistence length (26,27). If the attraction was much stronger than this the fibers would zipper together so strongly that sections of fiber would often be highly bent between contacts, leading to a far more extreme underestimate of the persistence length. If the attraction was much weaker than this the fibers would interact so weakly that the effect would be negligible compared to equilibrium fluctuation, leading to an estimate of the persistence length approximately equal to that obtained for fibers not in contact with one another. This attractive zippering force $f_{zip} \approx k_B T/\mu$m is very weak in chemical terms and likely negligible compared to the effect of bundling proteins like YgfE/ZapA found in vivo.

Comparison with tubulin microtubule persistence length

Our estimate of l_p for FtsZ is less than those available for tubulin, the prokaryotic homolog of FtsZ. Measurements of the persistence length of a microtubule assembled from pure tubulin by optical trap methods give a persistence

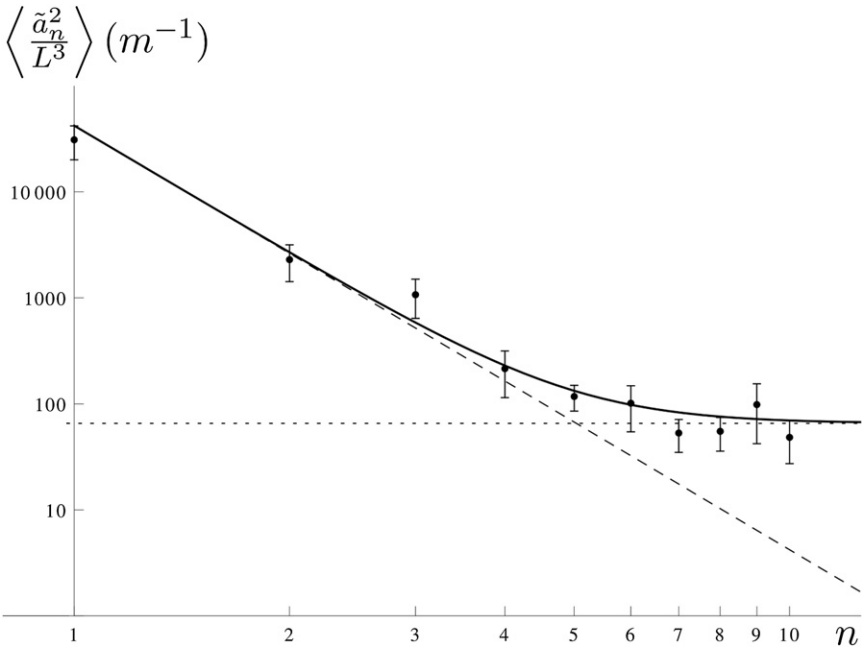

FIGURE 6 Plot showing $\langle \tilde{a}_n^2/L^3 \rangle$ for each Fourier mode n for nonisolated fibers. The experimental data from nonisolated FtsZ-GTP filaments are represented by circular markers with error bars corresponding to the mean ± standard error. The solid black line represents the theoretical model (strictly not applicable to nonisolated fibers) with our estimates of $l_p = 0.49\ \mu$m and $r = 3.61$ nm. The dashed and dotted asymptotes have the same meaning as in Fig. 4.

length for 14-protofilament microtubules of $l_p = 1.84$ mm (28). This corresponds to an estimated persistence length of $l_p = 4.03\ \mu$m for a single tubulin protofilament (29), which is approximately a factor of 3.5 greater than our estimate of the persistence length of FtsZ protofilaments. We also compare our estimate with the persistence length of a tubulin protofilament as given in another study of 2.8 μm (see Mickey and Howard (33)), based on an earlier estimate of microtubule persistence length of 5.2 mm (30). Again, the persistence length of tubulin protofilaments is estimated to be greater than our value for FtsZ protofilaments, this time by a factor of just over 2.5. Previous linear dichroism measurements of tubulin and FtsZ are consistent with tubulin being significantly stiffer than FtsZ (25,31).

Comparison with size of an *E. coli* cell

Our estimate of $l_p = 1.15 \pm 0.25\ \mu$m represents a persistence length comparable to the size of a typical *E. coli* cell, which is typically rod-shaped with an approximate length of 2 μm and diameter of 0.5 μm (32). Over these length scales, FtsZ filaments will behave like a semiflexible elastic rod. Thus, the persistence length may represent a balance between the need for fairly stiff fibers to facilitate ring assembly and fibers that are not so stiff that they impede division. It is also possible that the energy for Z-ring contraction may then be provided by the free energy released when the GTP in the filaments is hydrolyzed to GDP.

Implications for modeling cell division

Our estimate for l_p has impact in the context of some recent model studies of the Z-ring. A recent article by Allard and Cytrynbaum (14) describes a mathematical model for the force generated by a Z-ring both in vivo and in vitro, for which the rigidity of an FtsZ filament is an important parameter. In their study they assumed a value of 1.2×10^{-26} Nm^2 for the rigidity of an FtsZ protofilament, taken from a study on tubulin microtubules (33) on the basis of the sequence homology between FtsZ and tubulin. Using this value, their model predicts that the contraction of the Z-ring, driven by GTP hydrolysis, generates sufficient force (>8 pN) (34) to constrict the cell and hence permit division to take place. Although our estimate of the rigidity of FtsZ itself is lower by a factor of ~2.5, this probably only affects their model at the quantitative, rather than qualitative, level.

Another model study (15), which uses a value of 180 nm for the persistence length of an FtsZ protofilament, suggests that the initial force generated by the Z-ring is at most 2.8 pN, which is insufficient for Z-ring contraction to be the primary force generation mechanism for cell division. However, using our estimate of $l_p = 1.15\ \mu$m, which is greater than that used in (15) by a factor of ~6.4, their model would support forces of up to 17.9 pN, moving this threshold significantly over the minimum that they estimated was necessary to drive cell division (34). Our revised estimate of FtsZ rigidity therefore has potentially significant implications on the viability of various physics-based models of bacterial cell division.

SUPPORTING MATERIAL

Two tables are available at http://www.biophysj.org/biophysj/supplemental/S0006-3495(12)00088-4.

The authors thank Raul Pacheco-Gomez for his advice on FtsZ purification and polymerization, and Sarah Batson for her assistance and expertise in the laboratory during the purification process.

D.J.T. acknowledges the support of the Engineering and Physical Sciences Research Council via the Molecular Organisation and Assembly in Cells Doctoral Training Centre. M.S.T. acknowledges the support of an Engineering and Physical Sciences Research Council Leadership Fellowship EP/E501311/1. We are grateful to The Wellcome Trust for its generous support (grant reference: 055663/Z/98/Z) to the Imaging Suite at the University of Warwick.

REFERENCES

1. Hirota, Y., A. Ryter, and F. Jacob. 1968. Thermosensitive mutants of *E. coli* affected in the processes of DNA synthesis and cellular division. *Cold Spring Harb. Symp. Quant. Biol.* 33:677–693.
2. Errington, J., R. A. Daniel, and D. J. Scheffers. 2003. Cytokinesis in bacteria. *Microbiol. Mol. Biol. Rev.* 67:52–65.
3. Erickson, H. P., D. E. Anderson, and M. Osawa. 2010. FtsZ in bacterial cytokinesis: cytoskeleton and force generator all in one. *Microbiol. Mol. Biol. Rev.* 74:504–528.
4. Bi, E. F., and J. Lutkenhaus. 1991. FtsZ ring structure associated with division in *Escherichia coli*. *Nature.* 354:161–164.
5. Sun, Q., and W. Margolin. 1998. FtsZ dynamics during the division cycle of live *Escherichia coli* cells. *J. Bacteriol.* 180:2050–2056.
6. Mukherjee, A., and J. Lutkenhaus. 1994. Guanine nucleotide-dependent assembly of FtsZ into filaments. *J. Bacteriol.* 176:2754–2758.
7. Romberg, L., M. Simon, and H. P. Erickson. 2001. Polymerization of Ftsz, a bacterial homolog of tubulin: is assembly cooperative? *J. Biol. Chem.* 276:11743–11753.
8. de Boer, P., R. Crossley, and L. Rothfield. 1992. The essential bacterial cell-division protein FtsZ is a GTPase. *Nature.* 359:254–256.
9. Lu, C., M. Reedy, and H. P. Erickson. 2000. Straight and curved conformations of FtsZ are regulated by GTP hydrolysis. *J. Bacteriol.* 182:164–170.
10. Erickson, H. P. 2009. Modeling the physics of FtsZ assembly and force generation. *Proc. Natl. Acad. Sci. USA.* 106:9238–9243.
11. Erickson, H. P. 1997. FtsZ, a tubulin homologue in prokaryote cell division. *Trends Cell Biol.* 7:362–367.
12. Mingorance, J., M. Tadros, …, M. Vélez. 2005. Visualization of single *Escherichia coli* FtsZ filament dynamics with atomic force microscopy. *J. Biol. Chem.* 280:20909–20914.
13. Hamon, L., D. Panda, …, D. Pastré. 2009. Mica surface promotes the assembly of cytoskeletal proteins. *Langmuir.* 25:3331–3335.
14. Allard, J. F., and E. N. Cytrynbaum. 2009. Force generation by a dynamic Z-ring in *Escherichia coli* cell division. *Proc. Natl. Acad. Sci. USA.* 106:145–150.
15. Lan, G., B. R. Daniels, …, S. X. Sun. 2009. Condensation of FtsZ filaments can drive bacterial cell division. *Proc. Natl. Acad. Sci. USA.* 106:121–126.
16. Huecas, S., O. Llorca, …, J. M. Andreu. 2008. Energetics and geometry of FtsZ polymers: nucleated self-assembly of single protofilaments. *Biophys. J.* 94:1796–1806.
17. Rivetti, C., M. Guthold, and C. Bustamante. 1996. Scanning force microscopy of DNA deposited onto mica: equilibration versus kinetic trapping studied by statistical polymer chain analysis. *J. Mol. Biol.* 264:919–932.
18. Dajkovic, A., G. Lan, …, J. Lutkenhaus. 2008. MinC spatially controls bacterial cytokinesis by antagonizing the scaffolding function of FtsZ. *Curr. Biol.* 18:235–244.
19. Hörger, I., E. Velasco, …, M. Vélez. 2008. Langevin computer simulations of bacterial protein filaments and the force-generating mechanism during cell division. *Phys. Rev. E.* 77:011902.
20. Landau, L. D., E. M. Lifshitz, …, E. H. Dill. 1960. Theory of Elasticity: Vol. 7 of Course of Theoretical Physics. AIP, New York.
21. Chaikin, P., and P. Lubensky. 1995. Principles of Condensed Matter Physics. Cambridge University Press, Cambridge.
22. Wang, J. C., M. S. Turner, …, R. W. Briehl. 2002. Micromechanics of isolated sickle cell hemoglobin fibers: bending moduli and persistence lengths. *J. Mol. Biol.* 315:601–612.
23. Mukherjee, A., and J. Lutkenhaus. 1998. Purification, assembly, and localization of FtsZ. *Methods Enzymol.* 298:296–305.
24. Pacheco-Gómez, R., D. I. Roper, …, A. Rodger. 2011. The pH dependence of polymerization and bundling by the essential bacterial cytoskeletal protein FtsZ. *PLoS ONE.* 6:e19369.
25. Marrington, R., E. Small, …, S. G. Addinall. 2004. FtsZ fiber bundling is triggered by a conformational change in bound GTP. *J. Biol. Chem.* 279:48821–48829.
26. Jones, C. W., J. C. Wang, …, M. S. Turner. 2005. Measuring forces between protein fibers by microscopy. *Biophys. J.* 88:2433–2441.
27. Jones, C. W., J. C. Wang, …, M. S. Turner. 2003. Interactions between sickle hemoglobin fibers. *Faraday Discuss.* 123:221–236, discussion 303–322, 419–421.
28. Kikumoto, M., M. Kurachi, …, H. Tashiro. 2006. Flexural rigidity of individual microtubules measured by a buckling force with optical traps. *Biophys. J.* 90:1687–1696.
29. Armond, J. 2006. Modelling the force-generating properties of depolyerising microtubules. Master's thesis. University of Warwick, United Kingdom.
30. Gittes, F., B. Mickey, …, J. Howard. 1993. Flexural rigidity of microtubules and actin filaments measured from thermal fluctuations in shape. *J. Cell Biol.* 120:923–934.
31. Marrington, R., M. Seymour, and A. Rodger. 2006. A new method for fibrous protein analysis illustrated by application to tubulin microtubule polymerisation and depolymerisation. *Chirality.* 18:680–690.
32. Kubitschek, H. E. 1990. Cell volume increase in *Escherichia coli* after shifts to richer media. *J. Bacteriol.* 172:94–101.
33. Mickey, B., and J. Howard. 1995. Rigidity of microtubules is increased by stabilizing agents. *J. Cell Biol.* 130:909–917.
34. Lan, G., C. W. Wolgemuth, and S. X. Sun. 2007. Z-ring force and cell shape during division in rod-like bacteria. *Proc. Natl. Acad. Sci. USA.* 104:16110–16115.